frontiers | Frontiers in Mechanical Engineering

TYPE Original Research
PUBLISHED 10 November 2022
DOI 10.3389/fmech.2022.1013138

OPEN ACCESS

EDITED BY
Tiemin Xuan,
Jiangsu University, China

REVIEWED BY
Hu Wang,
Tianjin University, China
Yanzhi Zhang,
Jiangsu University, China
Zongyu Yue,
Tianjin University, China

*CORRESPONDENCE
Andrea Di Matteo,
a.di.matteo@tue.nl

SPECIALTY SECTION
This article was submitted to Engine and Automotive Engineering, a section of the journal Frontiers in Mechanical Engineering

RECEIVED 06 August 2022
ACCEPTED 03 October 2022
PUBLISHED 10 November 2022

CITATION
Di Matteo A, Bao H and Somers B (2022), Modeling Spray C and Spray D with FGM within the framework of RANS and LES. *Front. Mech. Eng* 8:1013138. doi: 10.3389/fmech.2022.1013138

Modeling Spray C and Spray D with FGM within the framework of RANS and LES

Andrea Di Matteo*, Hesheng Bao and Bart Somers

Power & Flow Group, Mechanical Engineering, Eindhoven University of Technology, Eindhoven, Netherlands

In this study, two different diesel-like igniting sprays are investigated: Engine Combustion Network (ECN) Spray C and D. In particular, this study focuses on the respective performances of the RANS and LES models to predict a turbulent, igniting spray using the OpenFOAM platform. The breakup model, discretization schemes, and case setups, including the combustion model, are kept constant in order to mitigate any potential effect on the simulation apart from intrinsic differences due to turbulence modeling. A classic κ-ε model is applied for the RANS approach, while a dynamic structure model is used to solve the momentum equation in the LES approach. The κ-ε model constants are tuned to obtain a suitable prediction of inert experiments. Both approaches exhibit a reasonable agreement with the inert experiments regarding the global spray characteristics, the liquid length, and the vapor penetration. However, the transient local properties, including the spatial distribution of mixture fraction variance and the species distributions, are not identical. For reacting conditions, the Flamelet Generate Manifold (FGM) model is adopted in both the LES and RANS simulations, using several enthalpy levels as the fourth dimension in the tabulation to account for local heat loss. The results show good agreement between the two turbulence models, in terms of liquid length, vapor penetration, and lift-off length, while a short ignition delay is registered for both sprays and turbulence frameworks. Turbulence–chemistry interaction (TCI) is considered by applying a presumed probability density function (β-PDF) to the mixture fraction, and is found to play a key role in the reproduction of species distribution in the domain.

KEYWORDS

spray modeling, ECN, spray C, spray D, FGM, RANS, LES

Introduction

Emission regulations have become increasingly strict in recent years. Climate change is driving clients and companies to focus on reducing pollutant emissions. This is also true for the transport sector, where for a long time and for a long time to come, the internal combustion engine has been the primary source of propulsion. Over the past 20 years, emission regulations have evolved to such levels that the study of each minute detail is necessary in order to comply with regulations. In this respect, Computational Fluid

Dynamics has become pivotal. However, several complexities arise in engine simulations, including turbulent flows in moving geometries, high pressure liquid injection (two phase flow), and chemical reactions (combustion), making it difficult to independently assess the quality of all sub-models.

For turbulent flow simulations of practical systems, a two model approach prevails, using a time averaging approach (Reynolds Averaged Navier-Stokes, RANS) and a spatial filtered approach (Large Eddy Simulation, LES). Each of these methods has its own advantages and disadvantages: RANS is extremely fast and widely used for industrial purposes; however, it is time averaged, meaning that the instant solution is not shown and therefore it is not precise enough to determine the relevant processes involved. LES is more precise, solving above a determined filter size and modeling everything below; however, it is computationally more expensive. Another level of simplification pertains to the choice of models that represent several physical processes occurring during injection and combustion, such as the spray breakup model, the evaporation model, and the combustion model itself. The latter model can be quite detailed; either all species are solved on runtime together with the turbulent flow or the solutions for both the combustion and turbulent flows are separated: the so-called tabulated model. The method used in this study is the Flamelet Generated Manifold (FGM) approach (Oijen van 2002), which is a tabulation method. This model simulates combustion for a canonical configuration (counterflow- and premixed-flame) and the results, in terms of controlled variables (primarily the mixture fraction and a progress variable), are stored in tables (manifolds) and are retrieved on runtime during the flow simulation. This way, only the transport equations for the chosen controlling variables are added to the simulation, instead of the equations for all species, significantly reducing the computational cost. The FGM model is based on the flamelet assumption (Peters, 1984): turbulent flame structures can be locally described by laminar flames. This assumption is widely adopted in spray combustion and more generally in engine combustion since the conditions for its validity are often verified in all types of internal combustion engines (excluding extremely high regimes). To be precise, the chemical timescale must be significantly smaller than the turbulent timescale; in other words, the flamelet can instantaneously adapt to the turbulent flow-field. Hence, a turbulent 3D flame can be decomposed and studied as an ensemble of 1D flames which can be simulated beforehand and the results of which are stored in tables. The turbulent-chemistry interactions are accounted for by using a presumed probability density function (PDF), applied to all the controlling variables. Several previous studies suggest that, depending on the case, neglecting the turbulent-chemistry interaction (TCI) may lead to flawed predictions during the combustion process (Pei et al., 2016; Bhattacharjee and Haworth, 2013; Desantes et al., 2020; Dahms et al., 2017).

Given the aforementioned assumptions in modeling the flow, injection, and combustion, a proper validation of full-engine simulations is of utmost importance. However, obtaining high-quality and high-resolution engine data is difficult. For this reason, a constant volume chamber is widely used to assess the quality of the CFD models. In this study, the so-called Spray C and Spray D introduced by the Engine Combustion Network (ECN) (ECN, 2022) are examined. The ECN is an international collaboration between several universities, institutes, and companies examining engine combustion. The collaboration aims to gather experimental data to provide a solid and complete characterization of the combustion process so that improvements in predictive CFD can be achieved. The most widely-studied setup is known as Spray A: a well-defined single orifice spray, injected into an ambient atmosphere with a temperature, pressure, and oxygen concentration closely resembling those found in diesel engines. An extensive database is available for inert and reacting conditions, detailing the liquid and vapor penetration, spatial fuel distribution (Pickett et al., 2011), ignition delay and lift-off length (Higgins and Siebers, 2001), and major species distribution (Maes et al., 2016; García-Oliver et al., 2017). In recent years, new single-hole nozzles with larger diameters were introduced, similar to those used in heavy-duty vehicle engines: Spray C and Spray D analyzed in this study. Both possess approximately the same diameter but differ in their proneness to cavitation. This phenomenon occurs when the local liquid pressure inside a nozzle (in general inside a tube) drops to a value that is lower than the liquid's vapor pressure, leading to a change in phase and thus a restricted fluid vein. Cavitation directly affects injection, generally increasing the spreading angle and modifying the ignition behavior and emissions (Pickett et al., 2011; Pastor et al., 2018; Westlye et al., 2016; García-Oliver et al., 2020). Spray C is designed to enhance cavitation, whereas Spray D uses a converging nozzle to avoid this phenomenon. This difference leads to distinct flow developments outside the nozzles; the reason spray C and D were chosen in this study.

The primary objectives of this study are: 1) to demonstrate that the FGM model can effectively represent the experimental data; 2) to evaluate any differences between the RANS and LES frameworks; 3) to analyze any differences in the combustion parameters for Spray C and Spray D; and 4) to outline the model parameters used and the reasons behind them.

This paper is divided into various sections: the Model Details section describes the combustion and breakup models applied and the relevant equations for both. An overview of the computational domain is also provided. This is followed by a section where inert cases are validated. Finally, the reacting cases are analyzed, and the results for both turbulent frameworks are compared to the experimental database.

Model Details

In the following equations, the tilde (~) used on a quantity (φ) represents, in case of the LES framework, a filtered quantity, whereas for the RANS approach it represents a Favre average.

FGM combustion model

As stated in the Introduction, the primary goal of this study is to assess the FGM combustion model using RANS and LES modeling to reproduce the spray behavior in the well-known benchmark cases Spray C and Spray D. The FGM model is a tabulated chemistry reduction approach that retrieves the relevant thermophysical properties from a pre-computed flamelet database, created beforehand by simulating physical-space laminar flames using the CHEM1D software (Somers LMT, 1994). In this study, the chemical mechanism comprising 54 species and 269 reactions (Yao et al., 2017) is adopted. In the FGM, the flame properties are stored in a database, parametrized by controlling variables, for which transport equations are solved in the 3D simulation. Subsequently, the solver, solving for the values of the controlling variables, directly applies the retrieved thermochemical properties. In general, for igniting FGM, the mixture fraction, Z, and a reaction progress variable, Y_c, are used as controlling variables. In this case, the mixture fraction in the flamelet simulation is defined by Bilger's approximation (Bilger et al., 1990) and its transport equation in turbulence is expressed as follows :

$$\frac{\partial \bar{\rho}\tilde{Z}}{\partial t} + \frac{\partial \bar{\rho}\tilde{u}_j\tilde{Z}}{\partial x_i} = \frac{\partial}{\partial x_i}\left[\mu_{eff}\frac{\partial \tilde{Z}}{\partial x_i}\right] + \overline{\dot{S}}_Z \tag{1}$$

Here, $\overline{\dot{S}}_Z$ is related to the injection of the liquid fuel and is coupled to the spray model. The progress variable, Y_C, is a linear combination of representative species given by :

$$Y_C = 1.5Y_{CH_2O} + 2.7Y_{HO_2} + 1.2Y_{H_2O} + 1.2Y_{CO_2} + 0.9Y_{CO} \tag{2}$$

Species are chosen to ensure that Y_C increases monotonically with the combustion process. Its transport equation is defined by :

$$\frac{\partial \bar{\rho}\tilde{Y}_c}{\partial t} + \frac{\partial \bar{\rho}\tilde{u}_i\tilde{Y}_c}{\partial x_i} = \frac{\partial}{\partial x_i}\left[\mu_{eff}\frac{\partial \tilde{Y}_c}{\partial x_i}\right] + \overline{\dot{\omega}}_{Y_c} \tag{3}$$

where $\overline{\dot{\omega}}_{Y_c}$ is the rate of production of the progress variable Y_C.

Both equations contain the term μ_{eff}, which, depending on the turbulence model adopted, can be written as follows. For the RANS :

$$\mu_{eff} = \mu + \mu_t \tag{4}$$

where μ_t in the $\kappa - \varepsilon$ model is defined as $\mu_t = \rho C_\mu \kappa^2/\varepsilon$, where C_μ is a constant. For the LES :

$$\mu_{eff} = \mu + \mu_{sgs} \tag{5}$$

where μ_{sgs} is the sub-grid scale dynamic viscosity, which in the present study is defined as $\mu_{sgs} = C_k \Delta k_{sgs}^{1/2}$, where C_k is a constant and k_{sgs} is the sub-grid kinetic energy defined by the transport :

$$\frac{\partial \bar{\rho}k_{sgs}}{\partial t} + \frac{\partial \bar{\rho}\tilde{u}_i k_{sgs}}{\partial x_i} = -\bar{\rho}\Gamma_{ij}\tilde{S}_{ij} - C_e\bar{\rho}\frac{k_{sgs}^{3/2}}{\Delta} + \frac{\partial}{\partial x_i}\left(\mu_{sgs}\frac{\partial k_{sgs}}{\partial x_i}\right) + \dot{W}_{s,sgs} \tag{6}$$

This type of sub-grid modeling is called a dynamic structure model; for further details, please refer to Bharadwaj et al. (2009), Tsang et al. (2019), and Bao et al. (2022).

In this work, the combustion model library is extended by adding the mixture fraction variance and the enthalpy. The former is added so that the turbulence–chemistry interaction is included, representing the influence of turbulence on combustion. Neglecting this effect would not only produce different distributions and species concentration peaks in the simulation (higher OH and NO peaks with the mass increased by a factor of two (Zhang et al., 2019)), but would also produce an extremely thin flame structure as well as longer ignition delays (Bhattacharjee and Haworth, 2013). It was discovered that ignition is retarded by considering the mixture fraction variance, whereas it is promoted by considering the progress variable variance (Zhang et al., 2019). Nevertheless, the latter has been neglected in this work so that the tables are not large and difficult to handle. Therefore, only the effect of mixture fraction variance is included, using a presumed β-shaped Probability Density Function (β-PDF) as discussed in several previous studies (Salehi and Bushe, 2010; Ge and Gutheil, 2006; Zhang et al., 2019). A simpler δ-function is used for the progress variable. The β-function PDF of a generical scalar, ϕ, is given by :

$$\tilde{P}(\phi) = \frac{\phi^{\alpha-1}(1-\phi)^{\beta-1}\Gamma(\alpha+\beta)}{\Gamma(\alpha)\Gamma(\beta)} \tag{7}$$

where the shape parameters, α and β, are determined by the mean and variance of the scalar ϕ, as follows :

$$\alpha = \tilde{\phi}\left[\frac{\tilde{\phi}\left(1-\tilde{\phi}\right)}{\widetilde{\phi''^2}}\right] \tag{8}$$

$$\beta = \left(1-\tilde{\phi}\right)\frac{\alpha}{\tilde{\phi}} \tag{9}$$

In order to apply this to the mixture fraction, a transport equation for $\widetilde{Z''^2}$ is solved as follows :

$$\frac{\partial \bar{\rho}\widetilde{Z''^2}}{\partial t} + \frac{\partial \bar{\rho}\tilde{u}_i\widetilde{Z''^2}}{\partial x_i} = \frac{\partial}{\partial x_i}\left[\mu_{eff}\frac{\partial \widetilde{Z''^2}}{\partial x_i}\right] + 2\mu_t\left|\frac{\partial \tilde{Z}}{\partial x_i}\right|^2 - \bar{\rho}\tilde{\chi} \tag{10}$$

where χ is the scalar dissipation rate, which describes the rate of molecular mixing between a fuel and an oxidizer. Since χ is an unclosed term in the above equation, it must be modeled; its

definition is vitally important to properly reproduce the distribution of species in the domain as this determines the variance of Z. Here, another difference between the RANS and LES turbulence models can be seen; the definition of the scalar dissipation rate. For the RANS model, it is assumed that the timescale for dissipation of the scalar variance is the same as the timescale for turbulence, ($\tau_t = \kappa/\varepsilon$), resulting in $\tilde{\chi}$ given by :

$$\tilde{\chi} = C_{\chi}\frac{\varepsilon}{\kappa}\widetilde{Z''^2} \tag{11}$$

where C_{χ} is a constant, typically defined as 2. For the LES model, $\tilde{\chi}$ can be decomposed into a resolved component, $\tilde{\chi}_{res} = C_{\chi}(\tilde{D}|\nabla\tilde{Z}|^2)$, where C_{χ} is also typically defined as 2, and a sub-grid component which is modeled following the local equilibrium hypothesis (Pierce and Moin, 1998) so that $\tilde{\chi}_{sgs} = \tilde{D}_{sgs}/\Delta^2\widetilde{Z''^2}$. As a result, the value of $\tilde{\chi}$ is given by :

$$\tilde{\chi} = C_{\chi}\left(\frac{\tilde{D}_{sgs}}{\Delta^2}\widetilde{Z''^2} + \tilde{D}\left(\frac{\partial\tilde{Z}}{\partial x_i}\right)^2\right) \tag{12}$$

In this study, enthalpy was added as an extra controlling variable in order to describe the effect of spray evaporation; the enthalpy departs from a pure adiabatic mixing line that would occur if two gases with different temperatures would mix. The implementation of this additional control variable leads to FGM tables with different levels of oxidizer enthalpies (instead of just one). As such, a transport equation is necessary for retrieval. In this study, the normalized enthalpy deficit, η_h, is introduced to retrieve the thermo-chemical space, relative to either the adiabatic state ($\eta_h = 0$), or (an a priori-defined) maximum heat loss state ($\eta_h = 1$) (for further information, please refer to Zhang *et al.* (2019)). The transport equation for enthalpy is given as :

$$\frac{\partial\bar{\rho}\tilde{h}}{\partial t} + \frac{\partial\bar{\rho}\tilde{u}_i\tilde{h}}{\partial x_i} = \frac{D\bar{p}}{Dt} + \frac{\partial}{\partial x_i}\left[\frac{\bar{\lambda}}{\bar{C}_p}\frac{\partial\tilde{h}}{\partial x_i} + \bar{\rho}\frac{\nu_t}{Pr_t}\frac{\partial\tilde{h}}{\partial x_i}\right] + \bar{S}_h \tag{13}$$

where h is the total enthalpy, $\bar{\lambda}$ and $\bar{C}_p$ represent the heat capacity and the thermal conductivity of the gas mixture, respectively, and ν_t and Pr_t are the turbulent kinematic viscosity and the turbulent Prandtl number, respectively.

Breakup model

In this work, droplet breakup is modeled using the Kelvin-Helmotz and Rayleigh-Taylor instabilities (Reitz, 1987). The KH component of the model is considered for the primary breakup phase. It assumes that a droplet with a radius r breaks up due to surface instability into smaller droplets with radii r_c, so that :

$$r_c = B_0\Lambda_{KH} \tag{14}$$

TABLE 1 Breakup model specifications for Spray C and Spray D.

	Spray C		Spray D
B_0		0.61	
B_1	7		5
C_{τ}		1	
Weber Limit		6	
Size Distribution		Rosin-Rammler	
Minimum Size		30.0e-6	
Maximum Size	200.0e-6		186.0e-6
Average Diameter		50.0e-6	

where Λ_{KH} is the wavelength at the maximum growth rate and B_0 is a constant. The smaller the parameter B_0, the smaller the droplet size after breakup. The rate of development of the parent droplet is calculated as follows :

$$\frac{dr}{dt} = \frac{r - r_c}{\tau_{KH}} \tag{15}$$

where τ_{KH} represents the breakup time and is given by :

$$\tau_{KH} = \frac{3.726B_1 r}{\Lambda_{KH}\Omega_{KH}} \tag{16}$$

where Ω_{KH} is the maximum growth rate of the wavelength Λ_{KH} and B_1 is a constant.

The RT component of the model is activated when secondary breakup of the droplet occurs; it predicts the instabilities on the droplet surface. If the wavelength is smaller than the droplet diameter, RT instabilities are growing on the droplet surface. The time for this growth is then compared with the breakup time as follows :

$$\tau_{RT} = \frac{C_{\tau}}{\Omega_{RT}} \tag{17}$$

where C_{τ} is a constant and Ω_{RT} is the wavenumber of the fastest growing instability.

The parameters for the KHRT model are reported in Table 1. It should be noted that the mass-based Rosin-Rammler distribution, with a minimum value equal to a fraction (1/5 or 1/6) of the nozzle diameter, was chosen in order to manage the size distribution.

Case description

As stated in the Introduction, the ECN cases examined in this study are Spray C and Spray D. The inert-condition cases are allowed to develop for 3 ms, whereas the reacting-condition cases develop for 5 ms. Injection starts at the beginning of the simulation. In all cases, a single-orifice injection of n-dodecane at 150 MPa is employed, and the ambient

TABLE 2 Specifications for ECN Spray C and Spray D (ECN, 2022).

	Spray C	Spray D
Fuel	n-dodecane	
Fuel Temperature (K)	363	
Injection pressure (MPa)	150	
Nominal Injection Diameter (μm)	200	186
Discharge Coefficient (-)	0.81	0.97
Ambient Temperature (K)	900	
Ambient Pressure (MPa)	6	
Inert Ambient Composition (% in mole)	O_2 : 0.00, N_2 : 89.71, CO_2 : 6.52, H_2O: 3.77	
Reacting Ambient Composition (% in mole)	O_2 : 15.00, N_2 : 75.15, CO_2 : 6.22, H_2O: 3.62	

conditions are identical (temperature, density, and species concentrations). The details are summarized in Table 2. The models and simulations are implemented and run in OpenFOAM software (OpenFOAM v7, 2020). The geometry, position of the injector (Figure 1), and all computational parameters are identical for both sprays modelled using both RANS and LES frameworks. The domain is represented by a cylinder with the injector on top, a square central refinement (for improved capturing of the spray and spatial distribution of the species), a total length of 140 mm, and a diameter of 47.612 mm. The extent of the domain is chosen such that it does not influence the flow. All boundaries apart from the ceiling are considered open (for details please refer to Table 3 where the most important boundary parameters are summarized).

Meshes are created using the blockMesh utility in OpenFOAM, which allows relatively straightforward creation

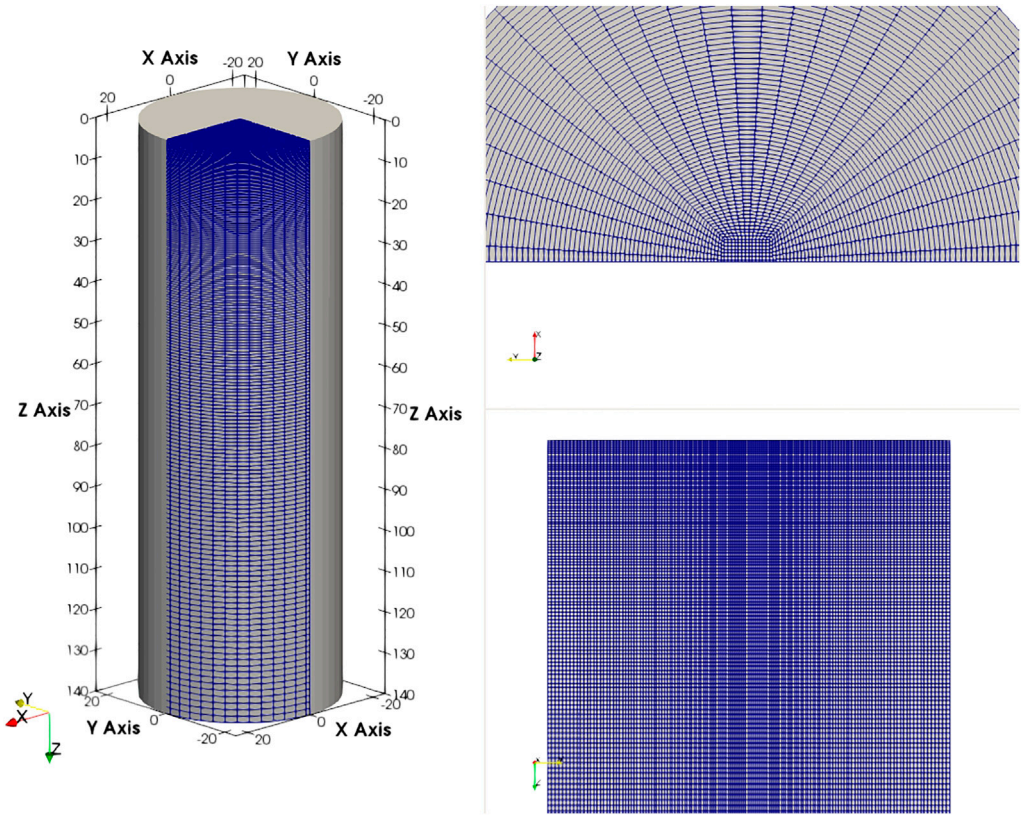

FIGURE 1
Cylinder dimensions and central refinement.

TABLE 3 Most important boundary settings.

	Boundary
Pressure	Dirichelet total pressure (outlet, lateral faces) Neumann zero gradient (inlet wall)
Temperature	Neumann zero gradient (all)
Velocity	Dirichelet non-backflow (outlet, lateral faces) Dirichelet fixed value (inlet)
Kinetic Energy	Neumann zero gradient (lateral faces, outlet) Wall function (inlet)
Density	Neumann zero gradient (all)

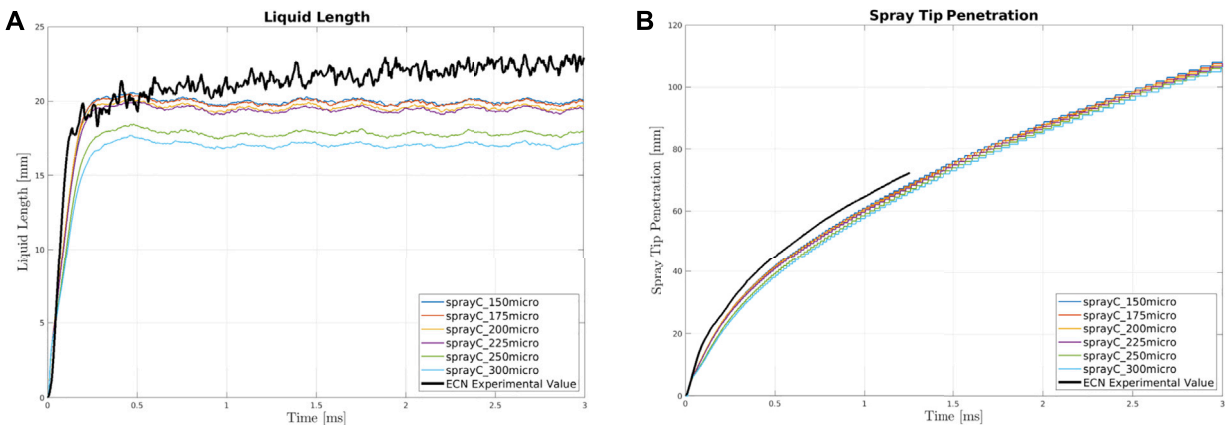

FIGURE 2
Liquid Length **(A)** and Spray Tip Penetration **(B)** for Spray C at various mesh dimensions.

of a structured mesh with simple geometries. All meshes, for both benchmarks and turbulence models, are created from a base cell size which represents the cell size on top of the central refinement squared region along the spray axis. This base cell is subsequently stretched towards the bottom and lateral walls of the cylinder, following a cell-to-cell expansion ratio. Different values for the base mesh size are used to investigate the convergence of the mesh.

Results and discussion

Model validation RANS

The major difference between the RANS and LES setups is the mesh; the RANS turbulence model allows the use of coarser meshes; the primary advantage of RANS simulations compared with LES models. Base cell sizes of 150 μm, 175 μm, 200 μm, 225 μm, 250 μm, and 300 μm are used for validation. The spray behavior for inert cases is analyzed in terms of the liquid length and the spray tip penetration. To assess the performances of both approaches, the inert cases are initially studied. The results from this will allow the mesh requirements to be set. Both the liquid length, defined as the distance from the nozzle containing 95% of the injected mass, and the spray tip penetration, defined as the farthest point from the injection point exhibiting a threshold value for fuel vapor mass concentration of 0.001 (Egüz et al., 2012), are compared with experimental results.

Since the principal goal of this work is a direct comparison of the RANS and LES models keeping the numerical set-up as similar as possible, a compromise, in terms of the performance achieved by all cases, was made in the choice of breakup model constants and discretization schemes. Thus, the analyzed vapor penetrations and liquid lengths perform relatively poorly in the single case, and the liquid length is unstable. The Appendix contains the vapor penetrations and liquid lengths for Spray C and Spray D in the RANS framework, providing an overview of any fine tuning required for each specific case [for the LES framework, refer to Bao et al. (2022)].

Spray C, inert

Figure 2 shows the results for Spray C.

As seen in Figure 2A the agreement with experimental data appears to be suitable for all mesh sizes, except for those

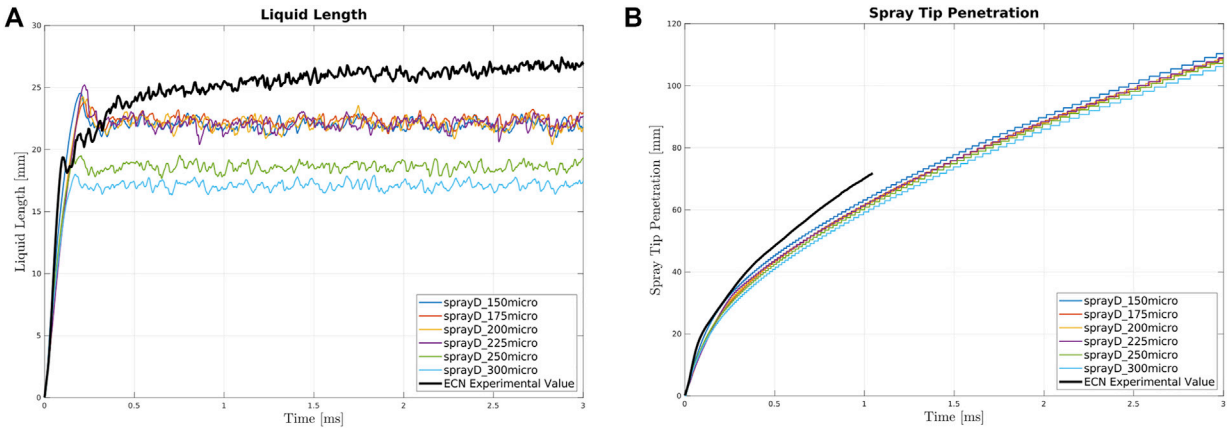

FIGURE 3
Liquid Length **(A)** and Spray Tip Penetration **(B)** for Spray D at various mesh dimensions.

with the largest base mesh sizes (250 μm and 300 μm), which exhibit considerably lower values. This relationship between the liquid length and the cell dimension is expected and is well-known. Indeed, the finer the mesh, the slower the evaporation since a smaller cell leads to faster saturation (KarŕHolm and Nordin, 2005), hence the longer liquid penetration for smaller cells. Typical liquid length behavior: an initial transient period followed by stabilization close to an average value (Siebers, 1998), is well reproduced. A plateau is reached after the two largest cell sizes, which are well below the experimental value. Further refinement of the base mesh size does not result in an improved liquid length compared with the experimental curve.

Figure 2B presents the spray tip penetration. Importantly, a suitable correspondence with the experimental data, close to the time when ignition generally occurs (0.58 ms for Spray C at 900 K) is observed. The agreement is not perfect since a distinct difference in the injection is observed at the initial stage. This issue seems to be correlated to the time step independency, which may be remedied by using a limiter on the turbulence length scale equal to the nozzle diameter, as suggested by KarŕHolm and Nordin (2005); however this is a matter for future studies. Furthermore, it should be noted that at the present time, an accurate trace of the spray tip penetration up to 3 ms is not available. Although the experimental value could be extrapolated to 3 ms, the result was not realistic; hence we avoided it in this study. However, all meshes appear to agree well with the experimental data, except the two coarsest which appear to display slower vapor penetrations; a direct consequence of the presence of additional liquid in the larger cell sizes. Since we must consider a good compromise in terms of computational effort hereafter, a mesh size of 225 μm (counting 747,643 cells) is chosen as the base mesh size for Spray C.

Spray D, inert

All above considerations for Spray C are also valid for Spray D. The geometry is identical, with the only differences being the nozzle diameter, the rate of injection, and the total mass injected. All other parameters are kept constant, and the six base sizes chosen for Spray C are also analyzed for Spray D. Figure 3 shows the liquid lengths and spray tip penetrations for Spray D.

A deviation from the experimental data is observed for the liquid length. After the first transient period, a clear peak in the instantaneous liquid length occurs; this is not observed in either Spray C or in the experimental data. This may be related to the numerical issue mentioned previously for the Spray C tip penetration, and requires further investigation. The mesh size trend highlighted in the Spray C section is also observed here; after an initial improvement in the performance upon refining the mesh, no further improvement in the average liquid length value occurs. Again, the coarsest meshes exhibit inferior performances.

The experimental ignition delay for Spray D is 0.59 ms and the difference between the experimental data and the model at this time is slightly larger than that observed for Spray C. Importantly, Spray D penetrates more rapidly than Spray C, in agreement with previous experimental observations (Pastor et al., 2018; Westlye et al., 2016). Similar to Spray C, the experimental data for Spray D do not reach 3 ms; extrapolation resulted in unrealistic results which were not used.

Since the two sprays do not require different base mesh sizes, a mesh size of 225 μm will be used for both hereafter, allowing coherent comparison of the two benchmarks.

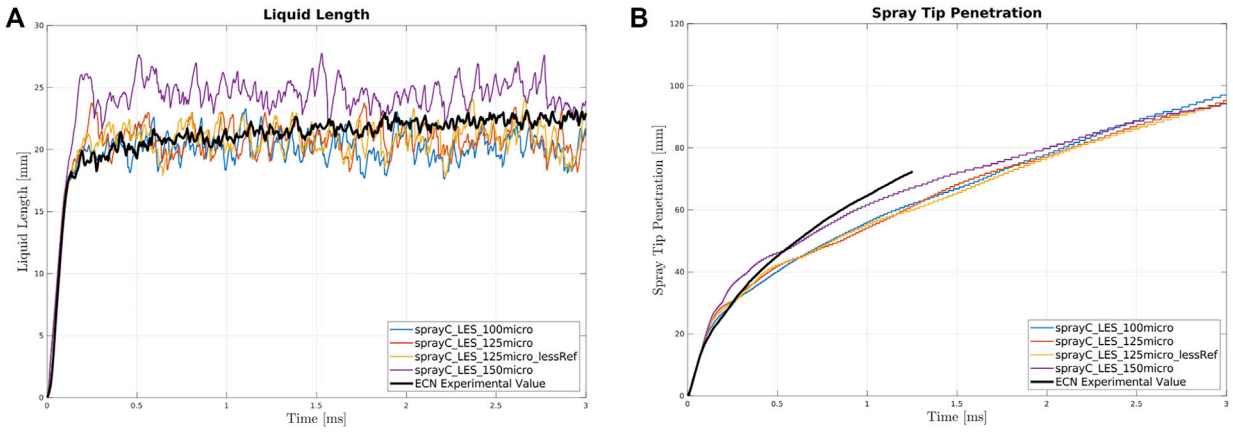

FIGURE 4
Liquid Length **(A)** and Spray Tip Penetration **(B)** for Spray C at various mesh dimensions.

Model validation LES

The above approach was also used here; however, a smaller number of base mesh sizes was analyzed. There are two reasons for this: firstly, the computational effort required here is higher since the meshes are approximately twice as large as the most refined mesh in the RANS analysis; secondly, one of the meshes analyzed here (named 125 μm lessRef) was used in a previous study (Bao et al., 2022). The validation in this previous study uses the same LES approach as in this work and the results in terms of spray tip penetration, liquid length, and distribution of mixture fraction and its variance are respectable. Therefore, this analysis begins from the reference dimension and adds one larger and one smaller base size in order to explore the mesh dependence.

Spray C, inert

In Figure 4, the liquid lengths and spray tip penetrations of Spray C are shown for the inert case, using four different base cell sizes: 100 μm, 125 μm, 125 μm (which is less refined in the radial direction), and 150 μm.

The liquid length graph shows small differences in the results where the trace stabilizes after the first transient element. In the RANS simulations, the difference in the various mesh sizes was significantly larger, with the two coarsest meshes performing noticeably worse than other sizes. Here, the only major deviation is observed for the coarsest mesh (150 μm), which yields a higher average liquid length value. This does not follow the relationship between the mesh size and the liquid length previously observed (KarrHolm and Nordin, 2005), and verified in the RANS validation section. The spray tip penetration agrees well with the relationship described above; the coarsest mesh presents the fastest evaporation. However, this is not an anomaly since more realizations are required to achieve improved statistical convergence. Another notable difference compared with the inert validation presented for the RANS model, is the considerably larger fluctuations in the average liquid length values. This is due to the nature of the two turbulence models: the RANS model provides an average of the fluctuations, whereas the LES model solves them (up to a defined size).

The first transient phase, in contrast to the RANS results, is perfectly reproduced by all meshes until approximately 0.15 ms, where differences begin to appear. Apart from the coarsest mesh, other meshes appear to behave similarly. Interestingly, although the first transient is reproduced, the maximum value reached at 3 ms is lower, even for the coarsest mesh which began with a significantly steeper slope. The turbulent fluctuations observed in the LES model significantly affect the spray, shortening the maximum length reached.

In conclusion, as far as Spray C simulations are concerned, the mesh size named 125 μm_lessRef (a larger mesh size in the radial dimension of the cylinder compared with the full 125 μm mesh) is chosen for further simulations. The mesh convergence for both the liquid length and the tip penetration appears to be achieved for the three most refined meshes. Therefore, in order to limit the computational effort required, and to possess a well-tested benchmark (Bao et al., 2022), the coarsest mesh (counting 2,755,584 cells) of the three most refined is used in the combustion analysis.

Spray D, inert

Figure 5 shows the inert results for Spray D; the same Spray C mesh base sizes were also analyzed here.

The observations made in the previous section can also be made here. Figure 5A clearly shows that the coarsest mesh performs worse than the others (150 μm); however, not to the extent observed for Spray C. Notably, all meshes perform worse in terms of the liquid length compared with Spray C. This can be

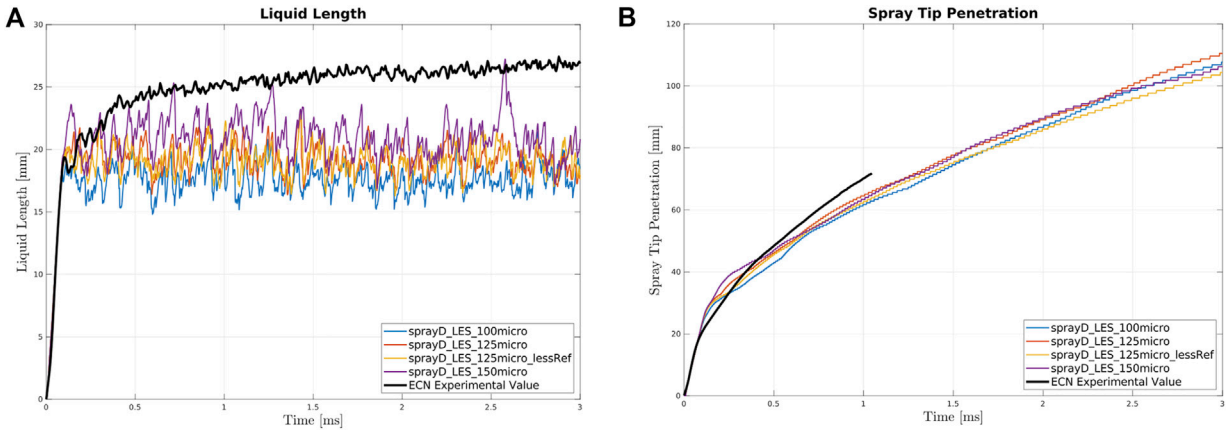

FIGURE 5
Liquid Length **(A)** and Spray Tip Penetration **(B)** for Spray D at various mesh dimensions.

explained by firstly considering the behavior previously highlighted in the RANS analysis of Spray D, which exhibits a peak after the first transient injection period and subsequently levels out to the average liquid length. The value obtained is lower than the experimental value. Secondly, the average experimental value is larger than that of Spray C. Consequently, the model clearly performs worse for Spray D than for Spray C.

For the spray tip penetration, the results are coherent with experimental results until approximately 1 ms. Notably, the model correctly reproduces the behavior previously observed for the RANS simulations; Spray D penetrates faster than Spray C. Moreover, the initial component of the penetration is perfectly reproduced; however, the initial change in slope provided by the simulation (~0.12 ms) occurs after the experimental data. This is unlike Spray C, where the considerably steeper change in slope occurs at the same time as the experimental data. The net result is that the penetration around the IDT (~0.5 ms) is significantly closer to the experimental value compared with Spray C. The Spray D penetration for all meshes is similar: the curve for the coarsest mesh is closer to the others than what is observed for Spray C.

Since the mesh performances appear to be decent in all cases, and since the use of one mesh for both benchmarks would lower the associated computational power, the same sized mesh as that chosen for Spray C is used for the remainder of the study.

Reacting cases analysis

In this section, the most important combustion performance indicators are presented. In particular, the ignition delay time (IDT), lift-off length (LOL), and species distribution along the flame are the key factors considered. These are analyzed for Spray C and Spray D and compared across the RANS and LES turbulence models.

Before proceeding with the analysis, a number of points should be considered: for the LES model, only one realization of the reacting case has been conducted. It has been shown previously (Bao et al., 2022) that more than one realization in the LES framework is required to obtain statistical convergence of certain quantities (OH and CH_2O mass fractions and LOL), but is not essential for others (mixture fraction and IDT). Thus, to save computational time, one realization of the global parameters (such as the IDT) is performed, similar to previous studies (Liu and Haworth, 2011).

Moreover, the transient development of the flame in both turbulence models as well as in all reacting cases is evaluated using so-called I_{xt}-plots (Maes et al., 2016). These plots show the radially integrated intensity of a certain species, x, along the spray axis x *versus* the time t (18):

$$I_{xt,i}(x,t) = \int \tilde{Y}_i(x,y,t)dy \tag{18}$$

where the intensity, $\tilde{Y}_i$, represents the mass fraction of the species and y is the radial dimension. IDT is defined as the time when 2% of the maximum obtained in the $I_{xt,OH}$-plot is achieved. This way, the variations in the local OH mass fractions (particularly large in the LES simulations) are smoothed by averaging. Another widely used definition of IDT is based on the time between the start of injection (SOI) and the time at which the greatest rate of maximum temperature increase is observed (Ong et al., 2021); this method gives consistent results (Bao et al., 2022). The same I_{xt} method is also used for the LOL calculation: LOL represents the location where the flame stabilizes and is calculated as the closest-to-nozzle location along the spray axis where 2% of the maximum $I_{xt,OH}$ value is achieved. Other thresholds for LOL can be found in the literature (from 2% to 50% (Pei et al., 2015; Wehrfritz et al., 2016; Som et al., 2011)); however, Pei et al.

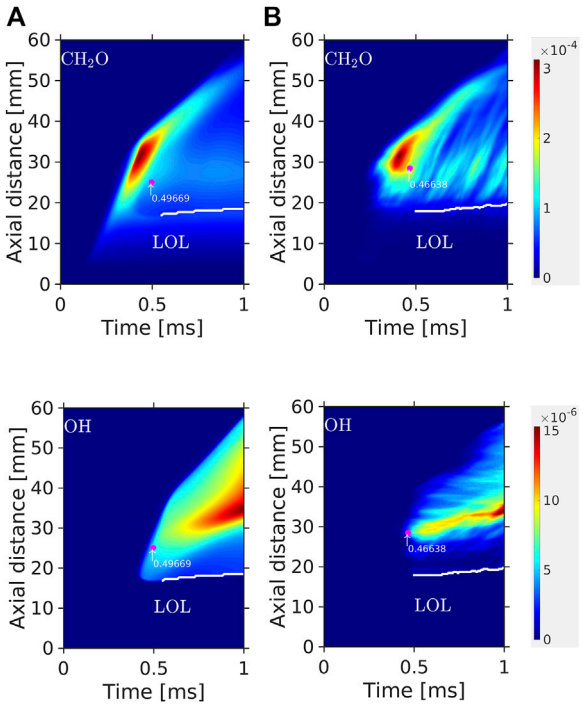

FIGURE 6
I_{xt}-plots for Spray C in the RANS **(A)** and LES **(B)** frameworks. The purple dot represents the IDT.

(2015) concluded that the consideration of different thresholds leads to minor changes.

It should be noted that OH typically indicates high-temperature chemistry, similarly, CH_2O is an indicator of low temperature combustion. We also analyze C_2H_2 as it is a precursor for soot emission.

Spray C, reacting

Figure 6 shows the I_{xt}-plots for Spray C. The red color represents high intensities (mass fraction percentage of the global maximum) of CH_2O and OH. The IDT is indicated by a purple dot and its value is specified. Finally, the instantaneous LOL value, evaluated from the $I_{xt,OH}$ fields, is also reported.

LES and RANS models present similarly-shaped CH_2O distributions and capture the separation between low- and high-temperature combustion in space and time, as noted previously (Bao et al., 2022), and experimentally observed for reacting sprays (Maes et al., 2016). Indeed, CH_2O formation occurs before the calculated IDT and is consumed before the beginning of the high-temperature zone, as shown in the $I_{xt,OH}$ plots. However, in the RANS simulation, CH_2O initially occurs noticeably closer to the nozzle and remains there until the high-temperature combustion begins and the LOL stabilizes. On the other hand, this does not occur in the LES model, and CH_2O is confined in a region closer to the LOL. Both simulations exhibit a precise division between the OH and CH_2O areas, as observed experimentally for reacting sprays (Maes et al., 2016). The OH intensity increases after the IDT, reaching a maximum in the latter stage, downstream compared with the stabilized LOL.

The highest OH intensity obtained in the LES model is observed in a narrower region, downstream from the LOL. The computed LOL values behave similarly in the two turbulence models; the LOL develops to below 20 mm shortly after the IDT; however, even after 1 ms, increases to approximately 22 mm where it stabilizes. These values compare well with the reported experimental value of 23.595 mm. Notably, the RANS simulation exhibits a LOL slightly lower than the LES model; this may be explained through the observation made by Pickett et al. (2005): a shorter cold flame (as in this case; CH_2O extends closer to the nozzle) results in a shorter LOL. Finally, the ignition delays for both turbulence models, 0.5 ms (RANS) and 0.47 ms (LES), are comparable to experimental values: 0.56 ms reported on the ECN website. This was also observed by Payri et al. (2019) and was attributed to the mechanism described by Yao et al. (2017).

Figure 7 presents a temporal evolution of Spray C. The visualization is divided into three groups representing three periods of time: the period prior to ignition (0.2–0.5 ms), the period directly after ignition (0.7–1.5 ms), and the quasi-steady period (2–3 ms). For each period three rows are provided; the second row represents the CH_2O, OH, and C_2H_2 species mass fractions. The first and third rows represent the temperature, variance of mixture fraction, and three iso-surfaces of mixture fraction (lean, stoichiometric, and rich). The LES model is presented at the top of the row while the RANS simulation is presented at the bottom of each row.

Clearly, as observed in the I_{xt}-plots above, low-temperature combustion (CH_2O) occurs from the beginning (0.2 ms) of the RANS simulation, whereas it is limited at that point in the LES model. The distribution of the variance of mixture fraction, $\widetilde{Z''^2}$, is different for each model. In the RANS model, the quantity is widely distributed for all time instances and becomes significant as the spray develops. The variance of mixture fraction is a direct result of the differences between the turbulence models. In fact, the source terms for the $\widetilde{Z''^2}$ equation [Eq. (10)] are different in the RANS and LES models, since the models that describe $\tilde{\chi}$, which acts as a sink-term, are different (Eqs. 11, 12). These directly influence the value of the variance, resulting in a smaller value for the LES model (for example, the maximum value for Spray D in the RANS model = 8.3e-3, while for Spray D in the LES model = 1.9e-3). In the LES model, the distribution of the low-temperature combustion immediately prior to IDT (0.4 ms) slightly shifts towards the downstream region, compared with the

RANS model (as also observed in the I_{xt}-plots but less prominent due to the integration procedure).

OH clearly appears after the IDT (0.5 ms) in the high temperature zone, close to the stoichiometric mixture fraction. Furthermore, the high-temperature ignition appears in the periphery of the spray plume, unlike what happens in smaller nozzles like Spray A where it appears at the spray tip. This is typical for such large nozzle sizes, as

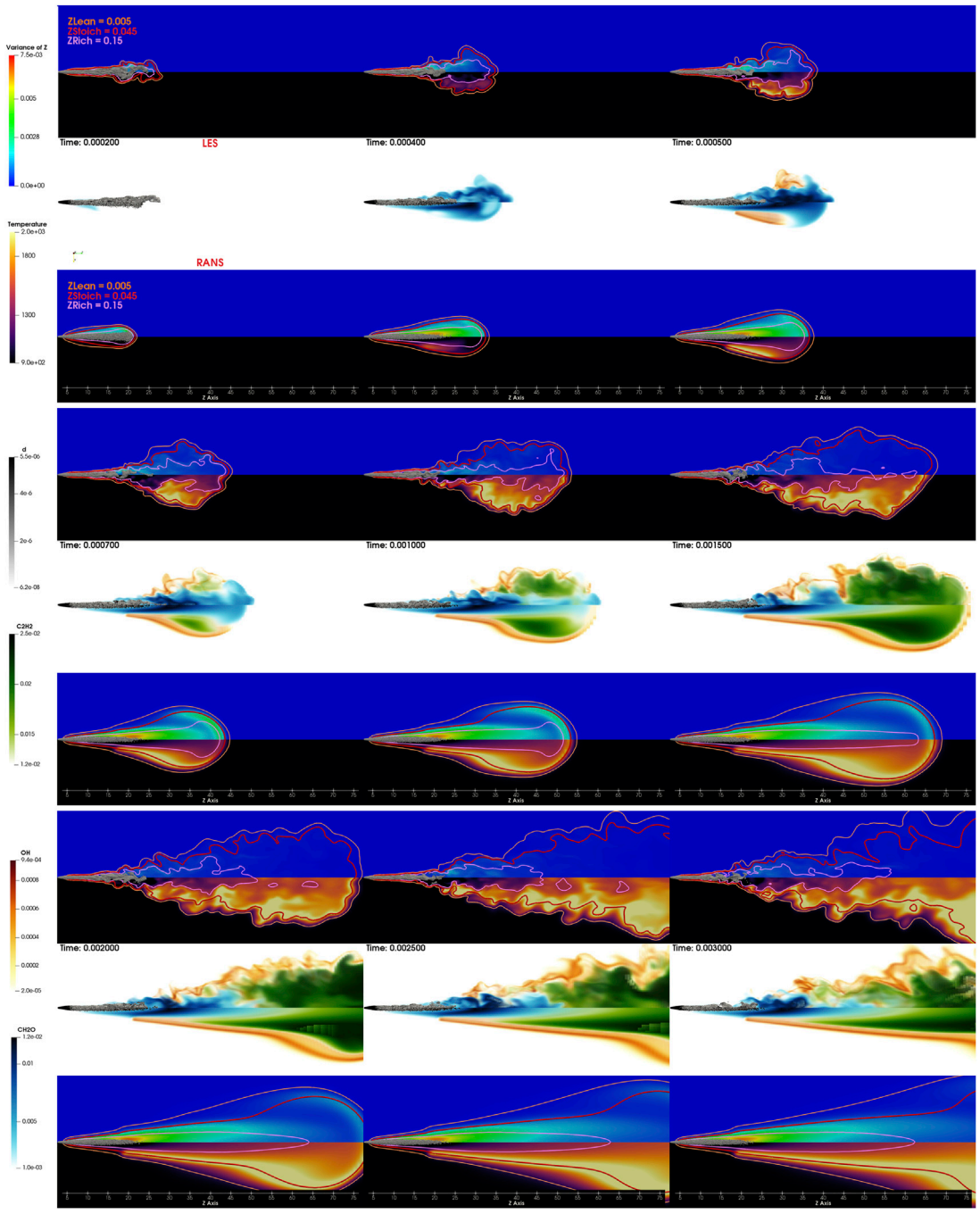

FIGURE 7
Spray C flame evolution from 0.2 ms to 3 ms. The image is divided into three parts: from 0.2 to 0.5 ms, from 0.7 to 1.5 ms, and from 2 to 3 ms. Each part is further divided into three: the central image represents OH, CH_2O, and C_2H_2 for the LES (upper) and RANS (lower) frameworks. The surrounding images are the temperature distribution, the variance of the mixture fraction, and three contours of the mixture fraction (lean, stoichiometric, and rich).

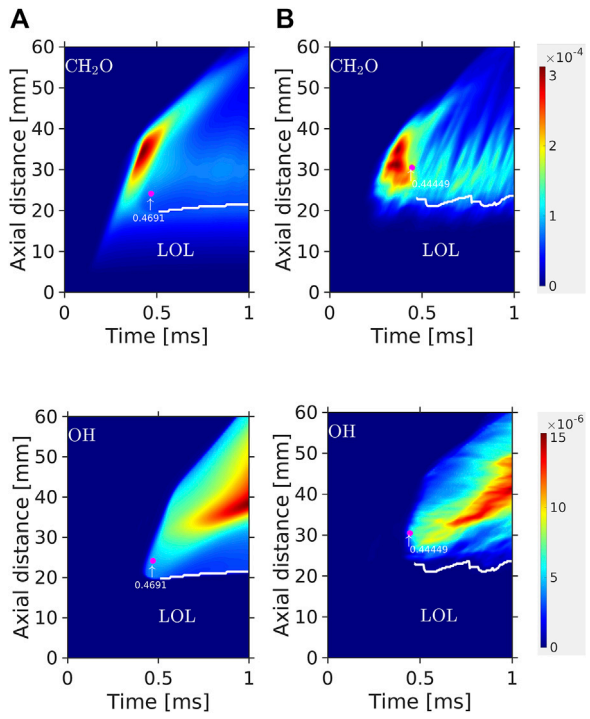

FIGURE 8
I_{xt}-plots for Spray D in the RANS **(A)** and LES **(B)** frameworks. The purple dot represents the IDT.

shown by García-Oliver et al. (2020). The distributions of C_2H_2, which is a product of rich combustion and is considered to be a soot precursor, appear within the flame core, close to the stoichiometric mixture fraction and the high-temperature zone in both simulations. In the RANS model, C_2H_2 initializes earlier (0.6 ms, not shown; the highest intensity is visible at 0.7 ms) than in the LES model. Afterwards, the maximum intensities of C_2H_2 are identical for both models, and move towards the spray tip, which becomes increasingly rich and hot. Interestingly, the high temperature area, straddling the contour of the stoichiometric mixture fraction, widens from 1 ms to 3 ms (the yellow region becomes increasingly wide). This trend is more visible in the RANS simulation but is present in the LES model, where, additionally, the flame is considerably more wrinkled and stretched by the stronger turbulent effects.

Spray D, reacting

Figure 8 shows the I_{xt}-plots for the Spray D reacting cases.

The observations here are similar to those made for Spray C. The low-temperature zone indicated by the CH_2O distribution in the RANS simulation is similar to that of Spray C, albeit slightly further from the nozzle; 15 mm for Spray C *versus* 18 mm for Spray D. Also for spray D, compared to the LES, CH_2O is present closer to nozzle. The intensity of CH_2O after the IDT is higher than that observed for the RANS model. This may however be due to the fact that only one realization is considered.

OH exhibits a larger high-intensity region compared with CH_2O, and the structure is more similar for the RANS and LES models compared with that observed for Spray C. Again, both turbulence models capture well the division between the low- and high-temperature flame regions. The CH_2O region still extends more towards the nozzle outlet in the RANS simulation compared with that observed in the LES model. The LOL predicted by the RANS simulation (21 mm) is shorter than that in the LES simulation (23.5 mm), similar to Spray C. The IDT is slightly longer in the RANS model (0.47 ms) than in the LES model (0.44s); however, both values are considerably shorter compared with the ECN experimental value of 0.56 observed for Spray C. It is important to underline that both approaches reproduce the experimental findings for the two sprays: Spray C exhibits a shorter LOL and Spray D a shorter IDT (Westlye et al., 2016). A remarkable difference between the turbulence models is the ignition location. In the RANS setup, it occurs closer to the nozzle than for the LES model, as also seen for Spray C. From this observation, ignition in the RANS framework is observed closer to the liquid length in a region richer in mixture fraction. This may yield higher soot production, in line with the higher amounts of the C_2H_2 precursor observed in the early stages of the RANS simulation for both sprays.

For clarity, Table 4 lists the values of the primary combustion parameters.

Figure 9 shows the flame evolution, similar to Figure 7. The observed behavior is comparable to above; CH_2O is present earlier in the RANS model, compared with the LES setup. A considerable difference is observed in terms of the variance of mixture fraction ($\widetilde{Z''^2}$); for Spray D it is even more significant. In the LES model, the only noticeable values of variance are present at the initial time instances.

TABLE 4 Most important combustion parameters for Spray C (left) and Spray D (right) from simulations and experiments.

Spray C	IDT (ms)	LOL (mm)	Spray D	IDT (ms)	LOL (mm)
RANS	0.49	19	RANS	0.47	21
LES	0.46	21	LES	0.44	23.5
Exp	0.56	23.6	Exp	0.56	25.9

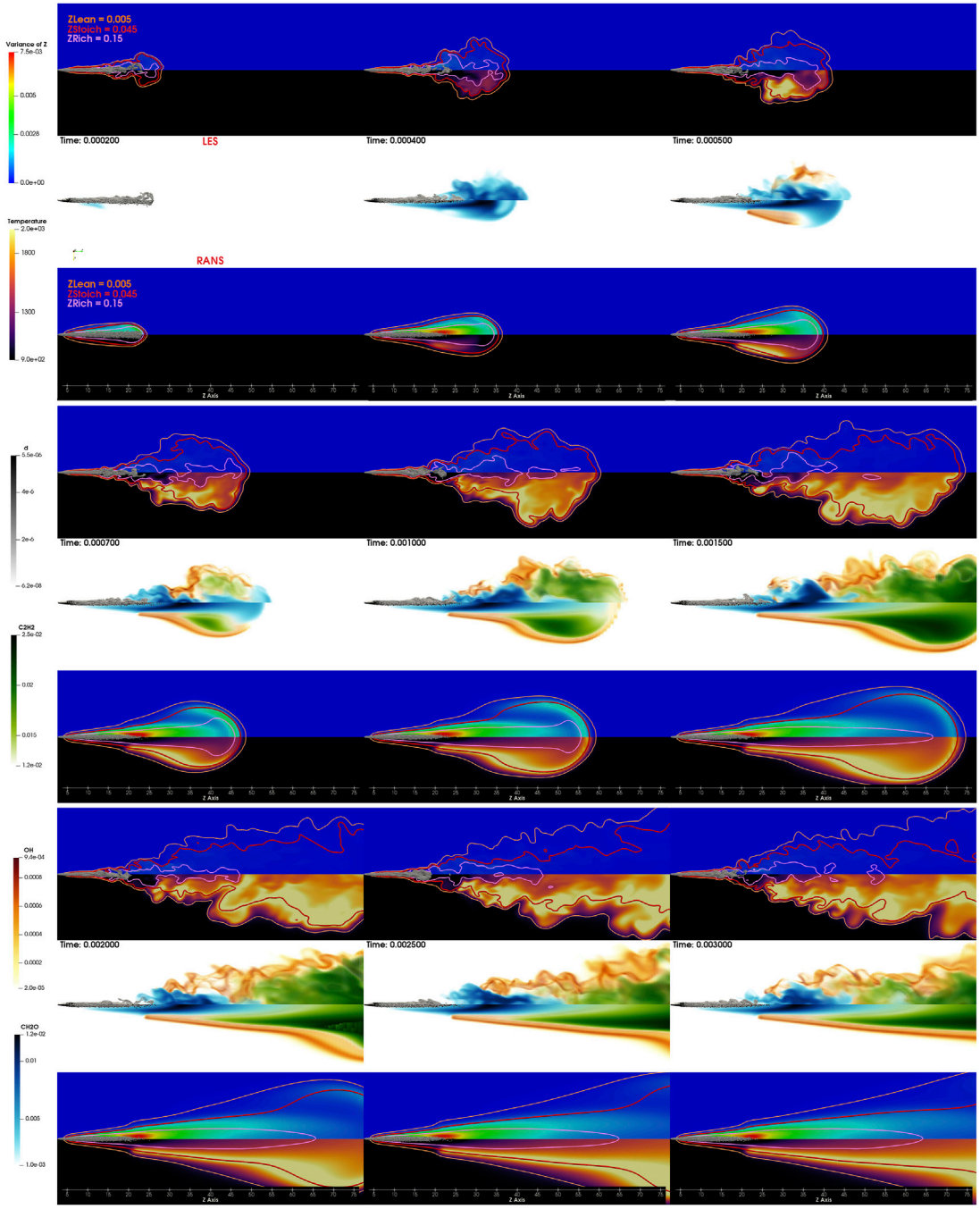

FIGURE 9
Spray D flame evolution from 0.2 ms to 3 ms. The image is divided into three parts: from 0.2 to 0.5 ms, from 0.7 to 1.5 ms, and from 2 to 3 ms. Each part is further divided into three: the central image represents OH, CH_2O, and C_2H_2 for the LES (upper) and RANS (lower) frameworks. The surrounding images are the temperature distribution, the variance of the mixture fraction, and three contours of the mixture fraction (lean, stoichiometric, and rich).

Furthermore, compared with Spray C, the variance intensity in the RANS model is even higher, for all chosen times, particularly close to the droplets. This is related to the fact that Spray D possesses a higher amount of injected mass compared with Spray C, so that the gradient of the mixture fraction, and accordingly, the variance of mixture fraction, are higher (Westlye et al., 2016). A difference in the high-temperature combustion region can also be seen. Along all

frames of the LES model for Spray D, the *OH* mass fraction is markedly higher than that of Spray C. This is also apparent in the I_{xt}-plots, where a broader and more intense *OH* region is observed, similar to the RANS simulation. This is related to the non-cavitating geometry used for Spray D, which allows a different evolution of the variance of mixture fraction in space, and involves retrieving different levels of species. Moreover, the variance smoothens the temperature: compared with Spray C, where the variance is lower, the widening of the high-temperature region is more prominent for Spray D, particularly at 1.5 and 2 ms. Similar to Spray C, the high-temperature ignition is located in the periphery of the spray plume, close to the stoichiometric mixture fraction region. C_2H_2 exists at all selected times; however, particularly in the LES model, the mass fractions are lower (maximum value for Spray D in the RANS simulation is 1.5e-2, while for the LES model it is 1.3e-2) and is located closer to the spray tip compared with Spray C (maximum value for Spray C in the RANS model is 1.6e-2, while for the LES model it is 1.7e-2). Maes et al. (2020) found that Spray C produces more soot than Spray D at 900 K, and *vice versa* at higher temperatures. Although the above observation follows the trend reported in the literature (higher amounts of soot precursor in Spray C at 900 K), further studies are required to confirm the opposite trend at higher temperatures. Moreover, the fact that the precursor is not a complete indicator of actual soot production should be considered.

Conclusion

In this study, the Spray C and Spray D ECN benchmarks were analyzed using the same solver (OpenFOAM) and the same combustion model (FGM). The performances of the RANS and LES turbulence models were compared, using the FGM combustion model with four-dimensional tabulation. The agreement with experiments, in terms of the liquid length and the spray tip penetration, are respectable for both turbulence models. For the reacting sprays, both the RANS and LES simulations reproduce the experimental observation that Spray C exhibits a shorter lift-off length, while the ignition delay for Spray D is shorter. In general, the ignition delays predicted by both turbulence models are shorter than the experimental values for both sprays. The RANS model predictions for the IDT are slightly longer than their LES counterparts, with ignition occurring closer to the nozzle outlet. The local characteristics of the markers for low-temperature chemistry (CH_2O), high-temperature chemistry (OH), and soot precursor (C_2H_2), predicted by both the RANS and LES models, are quite similar. The only large discrepancy between the LES and RANS models is observed in the distribution of the *OH* mass fraction for spray C.

In conclusion, both the RANS and LES models, coupled with the FGM combustion model, provide an excellent insight into the characteristics of the two ECN sprays, since the two methods provide similar results to experiments. The primary benefit of the LES model is the reproduction of the instantaneous flame shape and the species distribution, a natural consequence of a more precise turbulence chemistry interaction. Nevertheless, the RANS model remains a good choice in terms of efficiency since the required computational effort is lower and the primary parameter reproduction is close to that achieved by the LES model. This is important because it indicates the reliability of this turbulence model, which will be particularly useful for future studies where the computational domains will be significantly larger than that analyzed here.

Data availability statement

The raw data supporting the conclusion of this article will be made available by the authors, without undue reservation.

Author contributions

Corresponding author (ADM) is the first author, who wrote the article, performed simulations and post processing, coding. Second author (HB) helped in interpretation of results, coding and writing style. Third author (BS) is first author supervisor and helped in interpretation of results and writing style.

Funding

This project has received funding from the European Union's Horizon 2020 research and innovation program under grant agreement No 883753.

Conflict of interest

The authors declare that the research was conducted in the absence of any commercial or financial relationships that could be construed as a potential conflict of interest.

Publisher's note

References

Bao, H., Maes, N., Akargun, H. Y., and Somers, B. (2022). Large Eddy Simulation of cavitation effects on reacting spray flames using FGM and a new dispersion model with multiple realizations. *Combust. Flame* 236, 111764. doi:10.1016/j.combustflame.2021.111764

Bao, H., Kalbhor, A., Maes, N., Somers, B., and Van Oijen, J. (2022). Investigation of soot formation in n -dodecane spray flames using LES and a discrete sectional method. *Proc. Combust. Inst. S1540748922001183*. doi:10.1016/j.proci.2022.07.089

Bharadwaj, N., Rutland, C. J., and Chang, S. (2009). Large eddy simulation modelling of spray-induced turbulence effects. *Int. J. Engine Res.* 10, 97–119. doi:10.1243/14680874JER02309

Bhattacharjee, S., and Haworth, D. C. (2013). Simulations of transient n-heptane and n-dodecane spray flames under engine-relevant conditions using a transported PDF method. *Combust. Flame* 160, 2083–2102. doi:10.1016/j.combustflame.2013.05.003

Bilger, R. W., Stårner, S. H., and Kee, R. J. (1990). On reduced mechanisms for methane-air combustion in nonpremixed flames. *Combust. Flame* 80, 135–149. doi:10.1016/0010-2180(90)90122-8

Dahms, R. N., Paczko, G. A., Skeen, S. A., and Pickett, L. M. (2017). Understanding the ignition mechanism of high-pressure spray flames. *Proc. Combust. Inst.* 36, 2615–2623. doi:10.1016/j.proci.2016.08.023

Desantes, J. M., Garcia-Oliver, J. M., Novella, R., and Pachano, L. (2020). A numerical study of the effect of nozzle diameter on diesel combustion ignition and flame stabilization. *Int. J. Engine Res.* 21, 101–121. doi:10.1177/1468087419864203

ECN, Engine combustion network, 2022, (Available at: https://ecn.sandia.gov/).

Egüz, U., Ayyapureddi, S., Bekdemir, C., Somers, B., and de Goey, P., 2012. Modeling fuel spray auto-ignition using the FGM approach: Effect of tabulation method. SAE 2012 World Congress & Exhibition, Detroit, MI, April 24, 2012, pp. 2012-01–0157. doi:10.4271/2012-01-0157

García-Oliver, J. M., Malbec, L.-M., Toda, H. B., and Bruneaux, G. (2017). A study on the interaction between local flow and flame structure for mixing-controlled Diesel sprays. *Combust. Flame* 179, 157–171. doi:10.1016/j.combustflame.2017.01.023

García-Oliver, J. M., Novella, R., Pastor, J. M., and Pachano, L. (2020). Computational study of ECN Spray A and Spray D combustion at different ambient temperature conditions. *Transp. Eng.* 2, 100027. doi:10.1016/j.treng.2020.100027

Ge, H.-W., and Gutheil, E. (2006). Probability density function (PDF) simulation of turbulent spray flows. *At. Spr.* 16, 531–542. doi:10.1615/AtomizSpr.v16.i5.40

Higgins, B., and Siebers, D., Measurement of the flame lift-off location on dl diesel sprays using O H chemiluminescence, SAE Technical paper, 17. 2001.

KarŕHolm, F. P., and Nordin, N. (2005). "Numerical investigation of mesh/turbulence/spray interaction for diesel applications," in Paper i proceeding, 2005, Rio De Janiero, Brazil, May 11, 2005, 2005-01–2115. doi:10.4271/2005-01-2115

Liu, K., and Haworth, D. C. (2011). Development and assessment of POD for analysis of turbulent flow in piston engines. *SAE Tech. Pap.*, 2011-01–0830. doi:10.4271/2011-01-0830

Maes, N., Meijer, M., Dam, N., Somers, B., Baya Toda, H., Bruneaux, G., et al. (2016). Characterization of Spray A flame structure for parametric variations in ECN constant-volume vessels using chemiluminescence and laser-induced fluorescence. *Combust. Flame* 174, 138–151. doi:10.1016/j.combustflame.2016.09.005

Maes, N., Skeen, S. A., Bardi, M., Fitzgerald, R. P., Malbec, L.-M., Bruneaux, G., et al. (2020). Spray penetration, combustion, and soot formation characteristics of the ECN Spray C and Spray D injectors in multiple combustion facilities. *Appl. Therm. Eng.* 172, 115136. doi:10.1016/j.applthermaleng.2020.115136

Ong, J. C., Pang, K. M., Bai, X.-S., Jangi, M., and Walther, J. H. (2021). Large-eddy simulation of n-dodecane spray flame: Effects of nozzle diameters on autoignition at varying ambient temperatures. *Proc. Combust. Inst.* 38, 3427–3434. doi:10.1016/j.proci.2020.08.018

OpenFOAM v7 (2020). OpenFOAM v7. Available at: https://cpp.openfoam.org/v7/.

Pastor, J. V., Garcia-Oliver, J. M., Garcia, A., and Morales López, A. (2018). "An experimental investigation on spray mixing and combustion characteristics for spray C/D nozzles in a constant pressure vessel," in Proceedings of the International Powertrains, Fuels & Lubricants Meeting, Heidelberg, Germany, September 17, 2018, 2018-01–1783. doi:10.4271/2018-01-1783

Payri, F., García-Oliver, J. M., Novella, R., and Pérez-Sánchez, E. J. (2019). Influence of the n-dodecane chemical mechanism on the CFD modelling of the diesel-like ECN Spray A flame structure at different ambient conditions. *Combust. Flame* 208, 198–218. doi:10.1016/j.combustflame.2019.06.032

Pei, Y., Hawkes, E. R., Bolla, M., Kook, S., Goldin, G. M., Yang, Y., et al. (2016). An analysis of the structure of an n-dodecane spray flame using TPDF modelling. *Combust. Flame* 168, 420–435. doi:10.1016/j.combustflame.2015.11.034

Pei, Y., Som, S., Pomraning, E., Senecal, P. K., Skeen, S. A., Manin, J., et al. (2015). Large eddy simulation of a reacting spray flame with multiple realizations under compression ignition engine conditions. *Combust. Flame* 162, 4442–4455. doi:10.1016/j.combustflame.2015.08.010

Peters, N. (1984). Laminar diffusion flamelet models in non-premixed turbulent combustion. *Prog. Energy Combust. Sci.* 10, 319–339. doi:10.1016/0360-1285(84)90114-X

Pickett, L. M., Manin, J., Genzale, C. L., Siebers, D. L., Musculus, M. P. B., and Idicheria, C. A. (2011). Relationship between diesel fuel spray vapor penetration/dispersion and local fuel mixture fraction. *SAE Int. J. Engines* 4, 764–799. doi:10.4271/2011-01-0686

Pickett, L. M., Siebers, D. L., and Idicheria, C. A. (2005). "Relationship between ignition processes and the lift-off length of diesel fuel jets," in Proceedings of the Powertrain & Fluid Systems Conference & Exhibition, San Antonio, TX, October 24, 2005, 2005-01–3843. doi:10.4271/2005-01-3843

Pierce, C. D., and Moin, P. (1998). A dynamic model for subgrid-scale variance and dissipation rate of a conserved scalar. *Phys. Fluids* 10, 3041–3044. doi:10.1063/1.869832

Reitz, R. D. (1987). "Modeling atomization processes in high pressure vaporizing sprays," in *At. Sprays Technol* 3, 309–337.

Salehi, M. M., and Bushe, W. K. (2010). Presumed PDF modeling for RANS simulation of turbulent premixed flames. *Combust. Theory Model.* 14, 381–403. doi:10.1080/13647830.2010.489957

Siebers, D. L., 1998. Liquid-phase fuel penetration in diesel sprays. Technical paper, p. 980809. doi:10.4271/980809

Som, S., Longman, D. E., Lu, Z., Plomer, M., Lu, T., Senecal, P. K., et al. (2011). "Simulating flame lift-off characteristics of diesel and biodiesel fuels using detailed chemical-kinetic mechanisms and LES turbulence model," in Proceedings of the Internal Combustion Engine Division Fall Technical Conference (ICEF), Morgantown, WV, October 2, 2011, 12.

Somers LMT (Bart) (1994). *The simulation of flat flames with detailed and reduced chemical models*. Eindhoven, Netherlands: Doctor of Philosophy, Mechanical Engineering. doi:10.6100/IR420430

Tsang, C.-W., Kuo, C.-W., Trujillo, M., and Rutland, C. (2019). Evaluation and validation of large-eddy simulation sub-grid spray dispersion models using high-

fidelity volume-of-fluid simulation data and engine combustion network experimental data. *Int. J. Engine Res.* 20, 583–605. doi:10.1177/1468087418772219

Oijen van, J. A. (2002). *Flamelet-generated manifolds : Development and application to premixed laminar flames*. Eindhoven: Doctor of Philosophy, Mechanical Engineering. doi:10.6100/IR557848

Wehrfritz, A., Kaario, O., Vuorinen, V., and Somers, B. (2016). Large eddy simulation of n-dodecane spray flames using flamelet generated manifolds. *Combust. Flame* 167, 113–131. doi:10.1016/j.combustflame.2016.02.019

Westlye, F. R., Battistoni, M., Skeen, S. A., Manin, J., Pickett, L. M., and Ivarsson, A. (2016). "Penetration and combustion characterization of cavitating and non-cavitating fuel injectors under diesel engine conditions," in Proceedins of the SAE 2016 World Congress and Exhibition, Detroit, MI, April 12, 2016, 2016-01–0860. doi:10.4271/2016-01-0860

Yao, T., Pei, Y., Zhong, B.-J., Som, S., Lu, T., and Luo, K. H. (2017). A compact skeletal mechanism for n-dodecane with optimized semi-global low-temperature chemistry for diesel engine simulations. *Fuel* 191, 339–349. doi:10.1016/j.fuel.2016.11.083

Zhang, Y., Wang, H., Both, A., Ma, L., and Yao, M. (2019). Effects of turbulence-chemistry interactions on auto-ignition and flame structure for n-dodecane spray combustion. *Combust. Theory Model.* 23, 907–934. doi:10.1080/13647830.2019.1600722

Appendix

Figure A1 and Figure A2 reported vapor penetration and liquid length of Spray C and Spray D in RANS with fine tuning of the break-up model constants for the specific benchmark and turbulence model. The comparison is between the results obtained using the constants adopted in this work for compromise and the results obtained using constants obtained fine tuning each case alone.

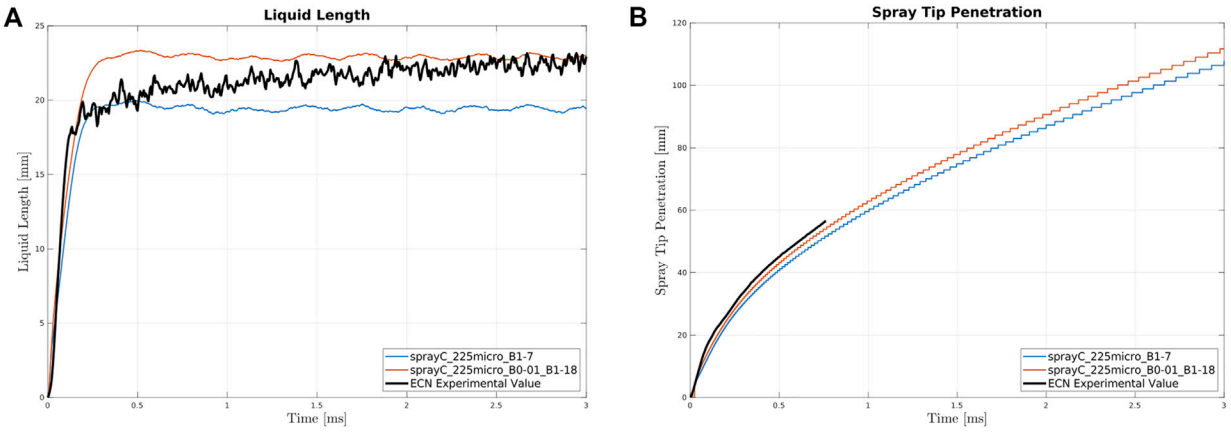

FIGURE A1
Liquid Length **(A)** and Spray Tip Penetration **(B)** for Spray C at varying break-up constants: in blue the one used in this work, in orange the optimized one.

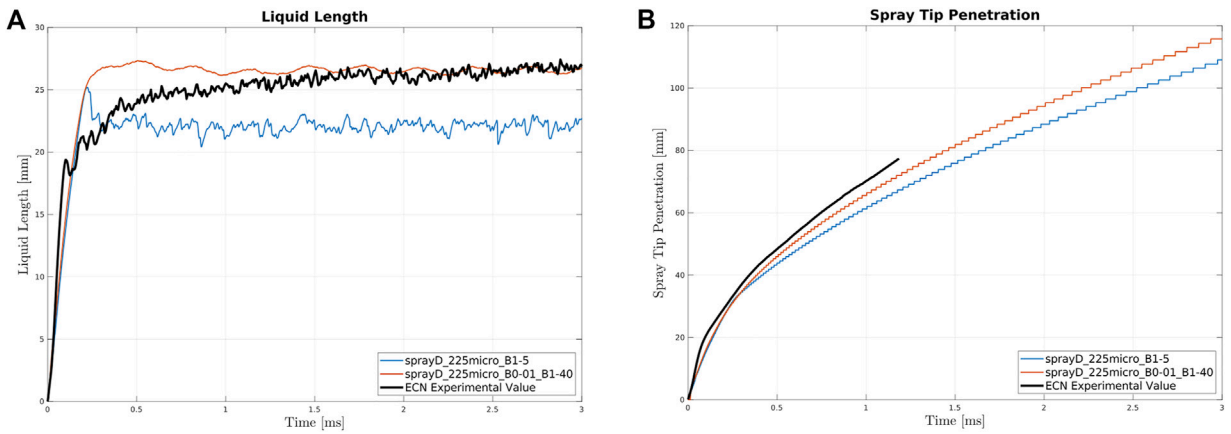

FIGURE A2
Liquid Length **(A)** and Spray Tip Penetration **(B)** for Spray D at varying break-up constants: in blue the one used in this work, in orange the optimized one.